Increased ATP citrate lyase affects maternal diabetes-induced neural tube defects by promoting the H3K27ac modification through the Gadd45g pathway

Baoling Bai (baoxiang8802@126.com)
Capital Institute of Pediatrics https://orcid.org/0000-0001-9505-5749

Zonghui Xiao
Capital Institute of Pediatrics

Zenzhen Zhou
Capital Institute of Pediatrics

Chunlei Wan
Capital Institute of Pediatrics

Dan Li
Capital Institute of Pediatrics

Lingyun Liu
Capital Institute of Pediatrics

Chunrong Sun
Capital Institute of Pediatrics

Yihua Bao
Capital Institute of Pediatrics

Huili Li
Capital Institute of Pediatrics

Qin Zhang
Capital Institute of Pediatrics

Research Article

Keywords: Maternal diabetes, Neural tube defects, ATP citrate lyase, Histone 3 lysine 27 acetylation, Gadd45g

Posted Date: May 2nd, 2022

DOI: https://doi.org/10.21203/rs.3.rs-1546141/v1

Abstract

Diabetes mellitus (DM) in early pregnancy increases the risk of neural tube defects (NTDs) in offspring. Enzyme-regulated histone acetylation has been reportedly linked to this pathological process. Few studies have focused on the intermediate acetyl-CoA, a substrate source of histone acetylation modification in maternal DM-induced NTDs. Here, we report that ATP citrate lyase (Acl), a metabolic enzyme of the glucose-related tricarboxylic acid cycle, has increased expression in DM-related NTDs of humans and mice, which induces acetyl-CoA accumulation and subsequently upregulates histone 3 lysine 27 acetylation (H3K27ac). Elevated H3K27ac reduces expression of genes for neural tube closure, Gadd45g and Ddit3. After inhibition of Acl, glucose-induced suppression of Gadd45g is alleviated by downregulation of H3K27ac both in vivo and in vitro, which is a possible mechanism of NTDs. Our results indicate that high glucose regulates NTD-related genes by increasing Acl and upregulating H3K27ac, which provide a novel pathological mechanism of DM-related NTDs.

Introduction

Pregestational diabetes mellitus (DM) (type 1 or 2) increases the risk for neural tube defects (NTDs) such as encephalocele in newborns [1–3]. Even if women take folic acid periconceptionally, women with pre-existing DM have 9-fold higher risk of fetal birth defects than those without DM [4, 5]. The discovery of insulin to control diabetes in the 1920s reduced the incidence of congenital malformed fetuses for maternal women with DM [1], but in recent years, the incidence of DM in women of childbearing age is increasing yearly, which may be due to the difficulty in achieving and maintaining glycemic control, and even a mother's momentary hyperglycemic exposure can lead to embryonic abnormalities [6]. Received modern pre-pregnancy care, for maternal DM, there still have a 2–5 fold higher incidence of offspring birth defects [2, 6]. Therefore, there is a great need for new therapeutics that inhibit the mechanisms underlying diabetic embryopathy.

It is well established that the main causative factors for maternal pregestational DM associated with NTDs are endoplasmic reticulum stress-induced oxidative stress and caspase activation-induced neuroepithelial cell apoptosis [7–9]. In recent years, histone acetylation, which is an epigenetic regulation, has emerged as a novel mechanism of DM-induced NTDs [10]. Our previous study showed that increased expression of histone acetyltransferase CREB-binding protein (CBP) is critical for upregulation of histone 4 lysine 5, 8, 12, and 16 acetylation in maternal diabetes-induced NTDs of mice *in vivo* and a neural stem cell model *in vitro*. Inhibition of CBP partially rescues the high glucose-induced excessive proliferation of neural stem cells [11]. In a mouse model of diabetic embryopathy, Yang et al. found that deacetylation enzymes Sirt2 and Sirt6 were suppressed and acetylation of histone 3 at lysine residues 56 (H3K56), H3K14, H3K9, and H3K27 was increased, whereas the potent sirtuin activator SRT1720 blocked high glucose-induced histone acetylation and reduced NTD formation [12]. Additionally, acetyltransferase Tip60 and deacetylation enzyme Sirt2 both regulate acetylation of the main neural tube closure gene MARCKS. Restoring Sirt2 expression in the developing neuroepithelium reversed maternal DM-induced cellular organelle stress, and apoptosis, and delayed neurogenesis to ameliorate NTDs [13]. These studies

mainly focused on the direct effects of histone acetylation-associated enzymes in maternal DM-induced NTDs. However, few studies have been conducted on the substrate required for acetylation, acetyl-CoA, a product of glucose metabolism.

Several studies have shown that adenosine triphosphate (ATP)-citrate lyase (ACL), which generates acetyl-CoA from mitochondrion-derived citrate, links cellular glucose metabolism to histone acetylation, indicating that glucose availability affects histone acetylation in an ACL-dependent manner [14, 15]. Das et al. showed that increased acetyl-CoA is regulated by ACL, which is used to acetylate histone H3 at MyoD regulatory regions, resulting in increased MyoD expression and improved muscle regeneration after injury [16]. By raising the acetyl-CoA concentration, ACL promotes H3K9/14 and H3K27 hyperacetylation in obesity-induced renal injury and upregulates several rate-limiting lipogenic enzymes and fibrogenic factors [17]. Additionally, high glucose promotes ACL expression and induces its translocation from the cytoplasm into the nucleus where ACL converts citrate to acetyl-CoA. Accumulation of acetyl-CoA markedly increases the modification levels of H3K9ac, H3K14ac and H3K18ac, leading to upregulation of fibrogenic genes, suggesting a critical role of ACL in epigenetic regulation of diabetic renal fibrosis [18]. Nevertheless, there is no report on whether ACL regulates histone acetylation in diabetes-induced NTDs.

In the present study, we investigated the expression of ACL protein and its potential effect on acetyl-CoA accumulation and histone 3 lysine acetylation (H3K27ac) regulation. We also explored an approach to alleviate acetyl-CoA by decreasing ACL expression with chemicals or siRNA technology to provide insights into the mechanisms of diabetic embryopathy and to help identify potential strategies to prevent diabetes-induced NTDs.

Methods

Human subjects

This investigation was approved by the Medical Ethics Committee of the Capital Institute of Pediatrics (No. SHERLLM2014002). Written informed consent was obtained from all participants in this study. The 100 NTDs and 100 normal control sample brain tissues were obtained from patients in the Lüliang area of Shanxi Province in northern China [19, 20]. Medically aborted fetuses which had been diagnosed with encephalocele by B-mode ultrasound in the early stages of pregnancy were subjected; Any fetuses displaying pathological malformations or intrauterine growth retardation were excluded from the control group; the summary of samples information were recorded in Table S1. In this study, 3 samples with the highest plasma glucose levels (the fasting blood glucose value□7 mmol/L) from 100 NTDs were selected, and 3 samples with normal glucose levels (□7 mmol/L) were selected from 100 controls. The summary of these six samples information were shown in Table S2.

Animal experiments

As described in our previous paper [11], diabetes female mice were induced in 7–9 week-old virgin FVB mice by twice intraperitoneal injections of 100 mg/kg body weight streptozotocin (STZ; S0130, Sigma),

which were dissolved in 100 mM sodium citrate buffer (C1013, Solarbio) at pH 4.5 and performed at an interval of 1 week. The fasting blood glucose value≥14 mmol/L after STZ treatment were confirmed as having diabetes. Female mice were treated with the same volume of vehicle (100mM sodium citrate buffer) and the blood glucose value ＜14 mmol/L, were included in the control group. The dams were then mated with 8–11-week-old male FVB mice. In addition, we established a rescue model, in 7-9 week-old, hydroxycitric acid (HCA) (90045-23-1, Sanherb, China), which can competitively inhibits ACL [21-23], was fed to STZ induced female mice 2g/kg/d for 4 weeks. The day that a vaginal plug was detected was considered day 0.5 of gestation, the dams were euthanized by CO2 for subsequent experiments. The study was approved by the Committee of Medical Ethics of the Capital Institute of Pediatrics (Beijing, China) (SYXK 2008–0011).

Grouping: On gestational day 8.5, embryos from maternal diabetic mice were grouped as DM; maternal mice fed with HCA and injected with STZ simultaneously, their embryos grouped as DM+HCA; embryos from control female mice were grouped in control group; Gestational day 14.5, at this stage, embryos with NTDs malformation can be clearly identified. Hence, we classified the NTDs fetus bred from diabetic mice to DM-NTDs group; the fetus bred from diabetic mice but without NTDs phenotype as DM group; embryos from maternal normal mice as control group. Details of the dissection information were shown in Table S3.

Glucose level detection

The human maternal plasma glucose content were detected by the laboratory department of our hospital. For mice, we collected the tail blood to measure by the blood glucose test strip, all tests were measured twice and the mean value was calculated.

Cell culture and glucose treatment

As described in our previous paper [11], NE4C cells (ATCC number: SCRC-CRL-2925™) [24] purchased from the Chinese Academy of Science, were cultured on plates pre-coated with 15 mg/ml poly L-lysine 2 h before passage in Eagle's MEM (Gibco) supplemented with 10% fetal bovine serum (FBS) (10099, Gibco), 1% GlutaMAX and 1% nonessential amino acids at 37 °C in 5% CO2. To stimulate high glucose exposure, cells were pre-incubated in serum-free medium for 24 h, and then 5mM (normal control) or 25mM (high) glucose (G7020, Sigma) were added in each group and both with FBS reintroduced, cells were further cultured 24 h for following experiments.

Acl overexpression and knockdown in NE4C cells

Acl wildtype plasmid obtained from Origene (LC420122) for Acl overexpression. Acl knockdown in NE4C cells were achieved by shRNA virus infection. Interfering sequence were designed by Sangon Biotech with pSGU6/GFP/Neo plasmid vector. A negative shRNA was used as a control. Cells were transfected with overexpression/shRNAs plasmids using the Lipo3000 reagent (Thermofisher) according to the manufacturer's instructions. In addition, we used an inhibitor of Acl: SB-204990 (154566-12-8, Sigma) at

0, 1, 5, 10 μmol/L for 24h. The overexpression and knockdown effects were verified by either western blotting or by immunofluorescence staining.

Histone extraction

Core histone proteins were extracted from NE4C cells/mice brain tissue using an acid extraction protocol [25]. The samples were first homogenized in lysis buffer (10 ml solution containing 10 mM Tris-Cl (pH 8.0), 1 mM KCl, 1.5 mM MgCl2 and 1 mM dithiothreitol (DTT)) and chilled on ice. Protease and phosphatase inhibitors were added immediately before cell lysis, and nuclei were isolated by centrifugation (1,500 g for 10 min). For the preparation of histones, nuclei were incubated with four volumes of 0.2 mol/L sulfuric acid overnight at 4 °C. The supernatant was precipitated with 33% trichloroacetic acid followed by centrifugation (12,000 g for 20 min). The obtained pellet was washed with cold acetone and subsequently dissolved in distilled water. The samples were stored at −80 °C before analysis.

Acetyl-CoA Assay

Brain tissues or cells were deproteinized by adding 200 μL of ice-cold 1 M perchloric acid (PCA) and homogenized thoroughly on ice using a Tissue-Tearor (Model 985370-395, Biospec Products Inc.). Then, the tissue was centrifuged at 10,000 *g* for 10 min to remove insoluble material. Acetyl-CoA level was measured with a kit (MAK039, Sigma). A 3M potassium bicarbonate solution was used to neutralize the supernatant until pH reached 6–8. Then, 10 μL sample and 40 μL buffer were added in the well, followed by a quenching and quench removal step. The fluorescence intensity was measured at $\lambda_{ex} = 535/\lambda_{em} = 587$nm by a machine (Thermoskan Flash, Thermo Scientific, USA).

In-solution tryptic digestion

As described in our previous paper [26], 50μg of total protein mixture was extracted from mice brain tissue and digested as follows. Disulfide bonds were reduced with 10mM (final concentration) DTT for 60 min at 37 °C. Then, alkylation was carried out by adding 40mM (final concentration) iodoacetamide for 60 min at room temperature in the dark. The alkylation reaction was quenched by treatment with 40mM DTT for 15 min. After diluting urea to less than 1 M with 25mM NH4HCO3, sequence-grade trypsin was added at a ratio of 1:50 (enzyme: total protein), and proteins were then digested at 37 °C for 24 h. The tryptic digestion was quenched by adding 1.0% trifluoroacetic acid, and the solution was then centrifuged at 13,000 g for 10 min to remove insoluble material. The supernatant was collected for subsequent experiments.

Identification and quantification of protein by Nano-HPLC/MS/MS

Nano-HPLC/MS/MS analyses were performed on a QE-HF mass spectrometer (Thermo Scientific, Bremen, Germany) equipped with an UltiMate 3000 RSLCnano System (Dionex, Germering, Germany). Full-scan MS spectra in the m/z range of 350–2000 were acquired using an Orbitrap. Twenty of the most

intense ions were isolated for MS/MS analysis. The raw data were processed using Proteome Discoverer (version 2.1.0.81, Thermo Scientific) by searching a database of human histones (www.uniprot.org, accessed October 2015) [27]. Peptides were generated from a semi-tryptic digestion with up to four missed cleavages, using carbamidomethylation of cysteines as a fixed modification and oxidation of methionines as a variable modification. Target histone lysine acetylation was searched at 42.0 Da [28]. The precursor mass tolerance was 10 ppm, and the product ions were searched at a tolerance of 0.025 Da. Peptide spectral matches were validated using a percolator based on q-values at a 1% false discovery rate (FDR). Modified peptides that passed the FDR were exported to a text file and processed by PRM. The area of the peaks was used to represent the number of modifications (as shown in our previous paper) [27].

Parallel reaction monitoring (PRM)

Raw data were searched against the corresponding histone database. The mass inclusion list included the mass, charge, polarity and time from the start and end. The full scan method was used as described above. The PRM method employed an Orbitrap resolution of 30,000 (at m/z 350) and a target automatic gain control value of 2×10^5. The precursor ions of each peptide were duplexed using ±0.8 m/z unit windows. Each sample was analyzed in triplicate (as shown in our previous paper) [27].

PRM data analysis

Protein quantification was manually processed within the Xcalibur Qual Browser (version 4.0.27.19; Thermo Fisher Scientific) using Skyline (version 3.5.0.9319; AB Sciex). In the Xcalibur Qual Browser, determination of the area under the curve of selected fragment ions was based on the presence of product ion signals within ±2.5 min of the expected retention time, with a mass error within ±5 ppm. In Skyline, .raw files were used as input to generate and extract the modified peptide normalized area at a 0.05 m/z ion match tolerance for each PRM spectrum (as shown in our previous paper) [27].

Western blotting (WB)

Total lysate total proteins or histone samples were resolved by 4-12% SDS-PAGE and subjected to western blot assays with the primary antibody: ACL (4332, Cell Signaling Technology (CST), 1:1000); Gadd45g(5174, CST, 1:1000); Sirt2 (12672, CST, 1:1000); Ddit3 (2895, CST, 1:1000); Gapdh (4970, CST, 1:1000) ; H3K4ac (ab176799, Abcam, 1:1000); H3K9ac (ab32129, Abcam, 1:1000); H3K14ac (ab52946, Abcam, 1:1000); H3K27ac (ab4729, Abcam, 1:1000); H3 (ab1791, Abcam, 1:1000). Followed by incubation with an anti-rabbit horseradish peroxidase-conjugated antibody (SC-2048, Zhongshan Jinqiao, 1:5000) and detection with a West Pico ECL kit (Thermo Scientific). The band intensities were determined using Image Lab software and expressed relative to Gapdh (for total proteins) / H3 (for histones).

ChIP-seq

A SimpleChIP® Enzymatic Chromatin IP Kit (9003, CST) was used for the ChIP assays, in accordance with the manufacturer's protocol. 4% Formaldehyde cross-linked chromatin was obtained from about 8×10^7 NE4C cells. Cross-linked chromatin was immunoprecipitated with antibodies to H3K27ac overnight at 4°C. Normal rabbit IgG were used as negative control. Immunoprecipitated DNA was analyzed by sequencing. Indepth whole-genome DNA sequencing was performed by BGI (www.genomics.org.cn, BGI, Shenzhen, China). The raw sequencing image data were examined by the Illumina analysis pipeline, aligned to the Mus musculus reference genome (UCSC, mm9) using Bowtie 2, and further analyzed by MACS (Model-based Analysis for ChIP-Seq; https://github.com/taoliu/MACS). Enriched binding peaks were generated after filtering through control input.

ChIP-qPCR

ChIP-qPCR analysis was performed using an ABI 7500 system (Applied Biosystems). The primers (Thermo Fisher Scientific, Inc.) used for ChIP-qPCRs are listed in **Table S4**. The relative enrichment of the histone modification was determined using the $2^{(\text{input-Ct})}{}_{\text{NTDs}} / 2^{(\text{input-Ct})}{}_{\text{Control}}$ method.

RNA extraction and RNA-seq analysis

Total RNA was extracted from cultured cells or frozen tissue samples at −80°C using TRIzol® (15596-026, Invitrogen). Library construction and sequencing were performed on a BGISEQ-500 by CapitalBio Technology (Beijing, China). Clean-tags were mapped to the reference genome and genes available at the Mice Genome. For gene expression analysis, the matched reads were calculated and then normalized to fragments per kilobase million (FPKM). The significance of the differential expression of genes was defined by the bioinformatics service of BGI according to the combination of the absolute value of log2 Ratio ≥ 1 and FDR ≤ 0.001.

RT-qPCR

RNA was reverse transcribed using a First Strand cDNA Synthesis kit (K1612; Beijing TransGen Biotech). The cDNA samples were analyzed using an Applied Biosystems 7500 Real-Time PCR system (Thermo Fisher Scientific, Inc.) and a 2X PCR UltraSYBR Mixture kit (CW0956; CWBIO) according to the manufacturer's protocol. The expression levels of the target genes were normalized to glyceraldehyde 3-phosphate dehydrogenase (Gapdh). The fold change in expression was determined using the 2-ΔΔCt method. The primer sequences designed using Primer 5 and synthetic by Sangon Biotech, Inc. are listed in Table S5. The PCR thermocycling steps were as follows: 95˚C for 10 min; then 40 cycles of 95˚C for 15 sec, 60˚C for 1 min; and 72˚C for 5 min.

Immunofluorescence staining (IF)

Cells were fixed in 4% paraformaldehyde for 15 min, and permeabilized in 0.1% Triton/PBS for 10 min in a 4 ℃ icebox. After incubation with 5% BSA for 1 hr at room temperature, primary antibody Acl (4332, CST, 1:150) was added. Secondary antibody goat anti-rabbit IgG H&L (Alexa Fluor 594) (ab150080,

Abcam, 1:500) was used. Nuclei were labeled with DAPI (P36935, Life technologies). Leica TCS SP8 confocal microscope was used to image the cells, and Image J software was used for analysis (Version 1.44)

Immunohistochemistry (IHC)

IHC studies were performed on 3μm sections obtained from brain tissues pre-fixation with 4% paraformaldehyde. Bioscience™ (00-4956-58, Invitrogen) were used for antigen retrieval. Then sections were blocked with 5% bovine serum albumin in PBS and incubated with the primary antibodies anti-Acl, anti-Gadd45g, anti-Ddit3 overnight at 4 ∘C. After washing with 0.1 M PBST, pH 7.4, 5 min, 3 times, antibodies were detected using the Polink-2 Plus polymer horseradish peroxidase detection system for goat primary antibodies (ZSGB-BIO) according to the manufacturer's instructions. Quality assessment was performed on each batch of slides by including a negative control in which the primary antibody was replaced by 10% normal goat serum to preclude nonspecific signals. The levels of Acl, Gadd45g and Ddit3 were analyzed by gray-scale analysis (ZEN 2012 ZEISS COMPANY).

Statistical analysis

All experiments were repeated at least three times. GraphPad Prism 8.0.1 (GraphPad Software, USA) was mainly used in the data analysis. Student's t-tests and one-way ANOVA analyses were used to determine the statistical differences among the groups. Data are presented as the mean ± SD. A p-value <0.05 was regarded as statistically significant.

Results

A high glucose environment upregulates ATP citrate lyase (ACL) protein expression

We retrospectively studied previously collected maternal plasma samples from 100 controls and 100 NTD fetuses. The analysis showed that the glucose content (mmol/L) in maternal plasma in the DM-NTD group was significantly higher than that in the control group (DM-NTDs: 5.53±0.37, Con: 4.57±0.23, p=0.047, n=100/group) (Table S1, Fig. 1A), which demonstrated that maternal hyperglycemia may be related to the occurrence of fetal NTDs.

To identify the ACL protein expression pattern, we first analyzed three maternal high blood glucose-related fetal NTDs and three fetal control brain tissues (Table S2, Fig. 1B). ACL protein exhibited increased expression compared with the control group (1.34±0.23-fold change, p=0.035, n=3/group) (Fig. 1C). Furthermore, we established a DM-induced NTD mouse model, including E8.5 (neural tube closure stage) (Fig. 1D) and E14.5 (Fig. 1E) embryos. WB and IHC showed that DM-induced fetal mice had inc

To identify the ACL protein expression pattern, we first analyzed three maternal high blood glucose-related fetal NTDs and three fetal control brain tissues (Table S2, Fig. 1B). ACL protein exhibited increased expression compared with the control group (1.34±0.23-fold change, p=0.035, n=3/group) (Fig. 1C). Furthermore, we established a DM-induced NTD mouse model, including E8.5 (neural tube closure

stage) (Fig. 1D) and E14.5 (Fig. 1E) embryos. WB and IHC showed that DM-induced fetal mice had increased Acl expression compared with control mice at E8.5 (1.26±0.02-fold change, p=0.045, n=5/group for WB; 1.56±0.04-fold change, p=0.026, n=3/group for IHC) (Fig. 1F, G; Fig. 5F, G). At E14.5, DM-induced non-NTD brain tissues had no significantly changed Acl expression compared with control groups (1.06±0.04-fold change, p=0.912, n=3/group), whereas in the DM-induced NTD group, Acl exhibited significantly enhanced expression compared with the control group (1.58±0.06-fold change, p=0.026, n=3/group) (Fig. 1F, H). PRM quantification supported these results (Fig. 1J, K; Table S6), Fig. 1I shows typical LC-MS/MS spectra of a tryptic peptide “SGGMSNELNNIISR” belonging to Acl. As a reference [12], Sirt2 (histone deacetylase) expression was also detected and its expression was significantly decreased in DM/DM-NTD group compared with control group at both E8.5 and E14.5 (Supplementary Fig. 1A, B) [12]. Abnormally high glucose levels in maternal blood, which leads to increased glucose transport to the embryo, is responsible for the teratogenic effects of maternal diabetes [29].Thus, we established a high glucose-induced neural stem cell (NE4C) model in vitro. The resulted showed a significantly increase of Acl with increasing glucose concentrations (Fig. 1L, Fig. 3D). Activation of ACL/Acl protein expression in vivo and in vitro induced by high glucose indicates that it may have a destructive effect on the regulation of downstream histone acetylation.

, p=0.026, n=3/group for IHC) (Fig. 1F, G; Fig. 5F, G). At E14.5, DM-induced non-NTD brain tissues had no significantly changed Acl expression compared with control groups (1.06±0.04-fold change, p=0.912, n=3/group), whereas in the DM-induced NTD group, Acl exhibited significantly enhanced expression compared with the control group (1.58±0.06-fold change, p=0.026, n=3/group) (Fig. 1F, H). PRM quantification supported these results (Fig. 1J, K; Table S6), Fig. 1I shows typical LC-MS/MS spectra of a tryptic peptide “SGGMSNELNNIISR” belonging to Acl. As a reference [12], Sirt2 (histone deacetylase) expression was also detected and its expression was significantly decreased in DM/DM-NTD group compared with control group at both E8.5 and E14.5 (Supplementary Fig. 1A, B) [12]. Abnormally high glucose levels in maternal blood, which leads to increased glucose transport to the embryo, is responsible for the teratogenic effects of maternal diabetes [29].Thus, we established a high glucose-induced neural stem cell (NE4C) model in vitro. The resulted showed a significantly increase of Acl with increasing glucose concentrations (Fig. 1L, Fig. 3D). Activation of ACL/Acl protein expression in vivo and in vitro induced by high glucose indicates that it may have a destructive effect on the regulation of downstream histone acetylation.

High glucose increases acetyl-CoA and the H3K27ac level in NE4C cells

Using the high glucose-treated NE4C cell model in vitro, we found that the level of acetyl-CoA increased with increases in the glucose concentration (Fig. 2A). We further analyzed several common histone acetylation modification sites related to NTDs, including H3K4ac, H3K9ac. H3K14ac and H3K27ac. Among them, the H3K27ac modification level was increased most significantly in the 25 mM glucose group compared with 5 and 12.5 mM glucose groups (Fig. 2B, C). Furthermore, we validated the results in the mouse model. The acetyl-CoA concentration in E8.5 fetal brain tissues of the DM group were significantly increased compared with that in the control group (Fig. 2D), similarly to the H3K27ac

modification level (Fig. 2E, F). At E14.5, only the DM-NTD group showed significant enhancement of the acetyl-CoA concentration and H3K27ac modification level compared with the control group (Fig. 2G–I). However, there was no significant difference in H3K4ac among the embryonic stages and groups (Fig. 2D–I). These results suggest that H3K27ac is a target effector in a high glucose environment.

ACL regulates the H3K27ac modification level

In a previous study, we found that both ACL expression and H3K27ac modification levels change under high glucose conditions. ACL promotes the level of histone acetylation by increasing acetyl-CoA synthesis. Therefore, we speculated that ACL regulates H3K27ac in a high glucose environment. We used gene overexpression and knockdown techniques in the in vitro NE4C cell model to test this hypothesis. First, 5 mM glucose-treated cells were transfected with a wildtype Acl gene plasmid (5 mM+WT group) or empty plasmid (5 mM+NC group). WB showed that Acl was significantly overexpressed in the 5 mM+WT group compared with 5 mM and 5 mM+NC groups, whereas no significant change was observed between 5 mM and 5 mM+NC groups (5 mM+WT vs 5m M+NC vs 5 mM: 1.59±0.04 vs 1.12±0.02 vs 1±0.01, $p < 0.021$, *p=0.035) (Fig. 3A). Immunofluorescence (IF) confirmed these results (Fig. 3D, E). Subsequently, we found that upregulated Acl protein expression was accompanied by the increased H3K27ac levels (5 mM+WT vs 5 mM+NC vs 5 mM: 1.79±0.14 vs 0.83±0.06 vs 1±0.02, $p < 0.05$) (Fig. 3A). Moreover, in the 25 mM glucose-cultured group, after knocking down Acl gene expression (25 mM + si-Acl-1 vs ’25 mM + si-Acl-2 group vs ’25 mM vs 5 mM: 1.25±0.02 vs 1.22±0.01 vs 1.45±0.01 vs 1±0.01, $p < 0.05$, $p < 0.025$) (Fig. 3B; Fig. 3D, E), the H3K27ac level was also decreased ($p < 0.05$) (Fig. 3B). Additionally, 25 mM glucose-cultured cells were treated with Acl-specific inhibitor SB-204990 at concentrations (0, 1, 5, and 10 μmol/L). As a result, SB-204990 did not affect Acl protein expression, but H3K27ac was downregulated in the 10 μM group compared with the 0 μM group ($p < 0.05$) (Fig. 3C).

DM mice were treated with HCA, an inhibitor of ACL enzymatic activity, and then E8.5 embryonic brain tissue was analyzed by WB. Compared with the DM group, Acl protein expression in the DM-HCA group showed no significant change, while H3K27ac was downregulated significantly ($p < 0.05$) (Fig. 3F–H). These results suggest that not only abnormal protein expression of Acl, but also inhibition of Acl enzymatic activity alters the H3K27ac modification in a high glucose environment.

H3K27ac regulates neural tube closure (NTC)-related genes Gadd45g and Ddit3 in maternal diabetes-induced NTDs

Next, we determined whether H3K27ac regulated the expression of genes with enriched peaks in ChIP-seq assays. We compared three E8.5 DM and three normal control brain samples, and obtained the H3K27ac enrichment level to the gene body (Table S7) and the mRNA expression level of genes by RNA-seq (Table S8, Supplementary Fig. 2). Furthermore, we combined and analyzed the ChIP-seq and RNA-seq data, screened 566 genes, which significantly changed in terms of binding ability to H3K27ac (>1.2-fold change, $p < 0.05$), and found significant changes in gene expression between DM and control groups (>1.3-fold change, $p < 0.05$) (Table S9, Fig. 4A). A four quadrant diagram showed a positive correlation between the binding level of H3K27ac to genes with the level of gene expression (Pearson’s

correlation=0.2127, p < 0.05) (Fig. 4B), that is, when the enrichment level of H3K27ac to gene decreases, the gene expression level may also decrease. A total of 566 genes were selected for further cluster analysis. The results showed that Control-1, Control-2, and Control-3 clustered to one group, and DM-1, DM-2, and DM-3 clustered to another group. These results indicated some common difference in DM-induced fetal mice (Fig. 4C). We then used the KEGG method to perform functional annotation clustering for the biological processes of the 566 genes. The results are shown in Table S10 and the top 20 signaling pathways are shown in Fig. 4D. Studies have shown that the MAPK signaling pathway is involved in the occurrence and development of NTDs [30, 31]. Therefore, we focused on this pathway. As shown in Fig. 4E, there were differential changes in the expression levels of 10 genes in the MAPK signaling pathway. Among them, only Gadd45g (Growth arrest and DNA damage 45) and Ddit3 (DNA-damage inducible transcript 3) have been reported to be related to the occurrence of mouse NTDs [32, 33].

In the DM group, the binding ability of four regions of the Gadd45g gene (Region 1: chr 13: 51845306–51846498; Region 2: chr 13: 51846675–51847029; Region 3: chr 13: 51848046–51848697; Region 4: chr 13: 51848923–51849244) to H3K27ac was significantly downregulated (p < 0.05), and Gadd45g gene expression was also significantly decreased in RNA-seq (DM vs Con: 3.88±0.54 vs 8.20±0.48, p < 0.05) (Fig. 4F). Similarly, the binding ability of a Ddit3 gene region (chr 10: 127290774-127296288) to H3K27ac was significantly downregulated and its gene expression was also significantly downregulated compared with the control group (DM vs Con: 5.08±0.47 vs 29.14±1.6, P < 0.05) (Fig 4G). These results suggest that NTD-related genes Gadd45g and Ddit3 are the effectors of DM to cause NTDs.

Abnormal Acl-H3K27ac-Gadd45g/Ddit3 pathway in DM-induced NTDs

In maternal E8.5 DM fetal mice, ChIP-qPCR confirmed decreases in H3K27ac enrichment of Gadd45g region 1/2 and Ddit3 region 2 (Fig. 5A, B). Additionally, DM+HCA fetuses exhibited upregulated enrichment of H3K27ac in Gadd45g region 1/2 compared with the DM group. Moreover, RT-qPCR validated the decreased mRNA expression of both Gadd45g and Ddit3 in the DM group, but there was no significant difference in DM+ HCA mice (Fig. 5C). Furthermore, we measured protein levels by WB (Fig. 5D, E) and IHC (Fig. 5F, G). The results all demonstrated significantly decreased expression of Gadd45g and Ddit3 proteins in DM. However, in the DM+HCA group, Gadd45g expression was partially but significantly rescued compared with DM mice.

To determine whether Gadd45g and Ddit3 were affected by ACL, we used the NE4C cell model and found that the binding ability of Gadd45g to H3K27ac was negatively correlated with the expression level of Acl for Gadd45g [Region 1: 5 mM *vs* 5 mM+ Acl (+) *vs* 25 mM *vs* 25 mM + Acl (-): 1 *vs 0.64 vs* 0.67 *vs* 0.97 ($p < 0.05$); Region 2: 5 mM *vs* 25 mM *vs* 25 mM+si-Acl: 1 *vs* 0.79 *vs* 0.75 *vs* 2.28 ($p < 0.05$) (Fig. 5H)] and its gene expression level [5 mM *vs* 5mM + Acl (+) *vs* 25 mM *vs* 25 mM + Acl (-): 1 *vs* 0.59 *vs 0.61 vs* 0.86 ($p < 0.05$) (Fig. 5J)]. For region 1 of the Ddit3 gene, its binding abundance to H3K27ac was as follows: 5 mM *vs* 5 mM+ Acl (+) *vs* 25 mM *vs* 25 mM + Acl (-): 1 *vs 0.72 vs* 0.81 *vs* 1.05 ($p < 0.05$) (Fig. 5I), and the RT-qPCR results were as follows: 5 mM *vs* 5 mM+ Acl (+) *vs* 25 mM *vs* 25 mM + Acl (-): 1 *vs* 0.63 *vs 0.74*

vs 0.81 ($p < 0.05$) (Fig. 5J). Finally, we used human samples for verification and found that mRNA expression of GADD45 was significantly downregulated in DM-NTDs (Fig. 5K). These results suggest that the increased Acl level in a high glucose environment upregulates H3K27ac, resulting in decreased expression of NTD-related genes Gadd45g and Ddit3 to induce NTDs, whereas after knockdown or inhibition of Acl, Gadd45g is partially rescued.

Discussion

Our study indicates that, in brain tissues of human DM-related NTD fetuses, maternal diabetes-induced NTDs mice *in vivo*, and high glucose-treated mouse neural stem cells *in vitro*, expression of ACL/Acl increases and is accompanied by accumulation of acetyl-CoA. Furthermore, the level H3K27ac was markedly increased and regulated by ACL. ChIP-seq combined with RNA-seq showed that both the binding ability of H3K27ac and gene/protein expression of NTD genes Gadd45g and Ddit3 were significantly reduced in DM-induced NTD mice and knockdown or inhibition of Acl partially rescued Gadd45g. In summary, increased ACL affects DM-induced NTDs by promoting the H3K27ac modification through the Gadd45g pathway.

Acl is the primary enzyme responsible for the synthesis of cytosolic acetyl-CoA and is expressed in many mammalian tissues, including the notochord, which is the early stage of neural tube development [34, 35]. Among 40 gene expressed in notochord cells, Acl was first to be expressed at the neural plate stage and its expression was restricted to notochord cells. After suppressing ACL functions with specific morpholinos, notochord cells failed to converge [36, 37]. It is noteworthy that the notochord as a source of inductive signals to pattern neural tube revealed that Acl has a major role in the neural tube development [34]. Our study confirmed that ACL had increased expressed in human maternal DM-related fetal NTDs and mouse DM-induced NTDs at E8.5 (neural tube closure stage) *in vivo*. In E9.5 neural stem cells *in vitro*, we also found that Acl expression was increased with the glucose concentration. Therefore, we next investigated its function.

Acl links glucose to histone acetylation [14]. Using a cell model, we verified that increased expression of Acl induced accumulation of acetyl-CoA as observed in DM-induced NTD mice. The enhancement of acetyl-CoA significantly upregulated H3K27ac, but not H3K4ac, H3K9ac, or H3K14ac. After knocking down Acl in 25 mM glucose-treated cells, H3K27ac was also decreased, suggesting a major regulatory role of Acl in H3K27ac. Increased H3K27ac has been observed in mouse diabetic embryopathy [12], but the mechanism of how H3K27ac changes and the possible downstream regulated genes in DM-induced NTDs remain unclear. Our previous study revealed abnormal H3K27ac regulation of apoptosisrelated genes in retinoic acid-induced mouse NTDs [38]. Decreased expression of Mark2 and Dvl1, which are NTD genes, was also regulated by H3K27ac in neural stem cells [39]. Thus, we hypothesized that H3K27ac may be involved in DM-induced NTDs through regulating NTD genes expression.

By combined analysis using ChIP-seq and RNA-seq, we found that increased H3K27ac in DM-induced NTDs of E8.5 mice further downregulated the expression of Gadd45 and Ddit3. In mammals, these genes

play important roles in the neural tube closure stage [33, 40, 41]. Murine Gadd45g have a conserved role in vertebrate neurogenesis, is mainly expressed in primary neuron precursors and post-mitotic neurons in sections and whole mouse embryos in in situ hybridizations [42]. In terms of how Gadd45 functions, in Gadd45-deficient mouse cells, Gadd45 appears to arrest the cell cycle at G2/M [43] and GADD45 proteins activates the p38 and/or c-jun N-terminal kinase pathway by directly binding to MAP three kinase 1/MAP/ERK kinase 4 in response to environmental stress, which further induces apoptosis [44, 45]. The Ddit3 (Gadd153) gene, a component of the CHOP-C/EBP complex, also interacts with Gadd45 and functions in combination. Moreover, knockdown of Ddit3 or Gadd45 abrogates apoptosis [46]. Therefore, decreased expression of Gadd45g and Ddit3 may destroy physiological apoptosis of neural cells in the early stage of neural tube closure, which causes excessive cell proliferation and participates in the occurrence of encephalocele induced by DM. This is consistent with the results of high glucose-induced cell proliferation in our previous study [11].

More recently, attention has focused on using antioxidants to ameliorate oxidative stress in NTDs induced by diabetic [47]. However, the antioxidants used to treat preeclampsia or cardiovascular disease, such as vitamins C and E, have yielded unsatisfactory results in humans and remain questionable [48]. Our study provides the opportunity to develop a novel treatments that block or disrupt Acl expression or appropriately activate the GADD45-related pathway to prevent birth defects in diabetic pregnancies.

Declarations

Acknowledgment

We thank Mitchell Arico from Liwen Bianji (Edanz) (https://www.liwenbianji.cn) for editing the language of a draft of this manuscript.

Author Contribution

Q.Z, H.L, and B.B conceived and designed the research; B.B, Z.X, Z.Z, C.W, D.L, and L.L performed the experiments; Y.B collected the human samples; B.B, Z.X, and C.S analyzed the data; B.B, Q.Z, and H.L edited the manuscript; Q.Z and H.L contributes equally to this work.

Funding

This study was supported by grants from the National Natural Science Foundation of China (Grant No. 81971397 and 82171652), and the Research Foundation of the Capital Institute of Pediatrics (Grant No. CXYJ-2021-02) to Qin Zhang. Baoling Bai was supported by the National Natural Science Foundation of China (Grant No. 81901167) and the Research Foundation of the Capital Institute of Pediatrics (Grant No. GZ-2021-04).

Availability of data and materials

All data generated or analyzed in this study are available in the published article.

Ethics Approval

Approval for this study was given by the Medical Ethics Committee of the Capital Institute of Pediatrics (No. 427 SHERLLM2014002) for human study, and No. SYXK 2008–0011 for animal experiments.

Consent to participate

Not applicable.

Consent for Publication

All authors have reviewed and approve the contents of the manuscript and consent for publication.

Competing Interests

The authors declare no competing interests.

References

1. Zabihi S, Loeken MR (2010) Understanding diabetic teratogenesis: where are we now and where are we going? Birth Defects Res A Clin Mol Teratol. 88:779–790. org/10.1002/bdra.20704. 10
2. Correa A, Gilboa SM, Besser LM, Botto LD, Moore CA, Hobbs CA, Cleves MA, Riehle-Colarusso TJ et al (2008) Diabetes mellitus and birth defects. Am J Obstet Gynecol. ; 199(3): 237 e231-239. doi: org/10.1016/j.ajog.2008.06.028
3. Tinker SC, Gilboa SM, Moore CA, Waller DK, Simeone RM, Kim SY, Jamieson DJ, Botto LD et al (2020) Specific birth defects in pregnancies of women with diabetes: National Birth Defects Prevention Study, 1997–2011. Am J Obstet Gynecol. ; 222(2): 176 e171-176 e111. doi: org/10.1016/j.ajog.2019.08.028
4. Oakley GP Jr (2012) Failing to prevent birth defects caused by maternal diabetes mellitus. Am J Obstet Gynecol 206(3):179–180. doi: org/10.1016/j.ajog.2011.12.019
5. Correa A, Gilboa SM, Botto LD, Moore CA, Hobbs CA, Cleves MA, Riehle-Colarusso TJ, Waller DK et al (2012) Lack of periconceptional vitamins or supplements that contain folic acid and diabetes mellitus-associated birth defects. Am J Obstet Gynecol 206(3):218e211–218e213. doi: org/10.1016/j.ajog.2011.12.018
6. Wu Y, Wang F, Reece E, A,Yang P (2015) Curcumin ameliorates high glucose-induced neural tube defects by suppressing cellular stress and apoptosis. Am J Obstet Gynecol. ; 212(6): 802 e801-808. doi: org/10.1016/j.ajog.2015.01.017
7. Garcia-Sanz P, Mirasierra M, Moratalla R, Vallejo M (2017) Embryonic defence mechanisms against glucose-dependent oxidative stress require enhanced expression of Alx3 to prevent malformations during diabetic pregnancy. Sci Rep 7(1):389. doi: org/10.1038/s41598-017-00334-1

8. Chen X, Zhong J, Dong D, Liu G, Yang P (2017) Endoplasmic Reticulum Stress-Induced CHOP Inhibits PGC-1α and Causes Mitochondrial Dysfunction in Diabetic Embryopathy. Toxicol Sci 158(2):275–285. doi: org/10.1093/toxsci/kfx096
9. Chen X, Shen WB, Yang P, Dong D, Sun W, Yang P (2018) High Glucose Inhibits Neural Stem Cell Differentiation Through Oxidative Stress and Endoplasmic Reticulum Stress. Stem Cells Dev 27(11):745–755. doi: org/10.1089/scd.2017.0203
10. Banik A, Kandilya D, Ramya S, Stünkel W, Chong YS, Dheen ST (2017) Maternal Factors that Induce Epigenetic Changes Contribute to Neurological Disorders in Offspring. Genes (Basel) 8(6). doi: org/10.3390/genes8060150
11. Bai B, Zhang Q, Wan C, Li D, Zhang T, Li H (2018) CBP/p300 inhibitor C646 prevents high glucose exposure induced neuroepithelial cell proliferation. Birth Defects Res 110(14):1118–1128. doi: org/10.1002/bdr2.1360
12. Yu J, Wu Y,Yang P (2016) High glucose-induced oxidative stress represses sirtuin deacetylase expression and increases histone acetylation leading to neural tube defects. J Neurochem 137(3):371–383. doi: org/10.1111/jnc.13587
13. Yang P, Xu C, Reece EA, Chen X, Zhong J, Zhan M, Stumpo DJ, Blackshear PJ et al (2019) Tip60- and sirtuin 2-regulated MARCKS acetylation and phosphorylation are required for diabetic embryopathy. Nat Commun 10(1):282. doi: org/10.1038/s41467-018-08268-6
14. Wellen KE, Hatzivassiliou G, Sachdeva UM, Bui TV, Cross JR, Thompson CB (2009) ATP-citrate lyase links cellular metabolism to histone acetylation. Science 324(5930):1076–1080. doi: org/10.1126/science.1164097
15. Zhao S, Torres A, Henry RA, Trefely S, Wallace M, Lee JV, Carrer A, Sengupta A et al (2016) ATP-Citrate Lyase Controls a Glucose-to-Acetate Metabolic Switch. Cell Rep 17(4):1037–1052. doi: org/10.1016/j.celrep.2016.09.069
16. Li HSartorelliVATP, Citrate Lyase (2018) A New Player Linking Skeletal Muscle Metabolism and Epigenetics. Trends Endocrinol Metab 29(4):202–204. doi: org/10.1016/j.tem.2018.01.006
17. Chen Y, Deb DK, Fu X, Yi B, Liang Y, Du J, He L, Li YC (2019) ATP-citrate lyase is an epigenetic regulator to promote obesity-related kidney injury. Faseb j 33(8):9602–9615. doi: org/10.1096/fj.201900213R
18. Deb DK, Chen Y, Sun J, Wang Y, Li YC (2017) ATP-citrate lyase is essential for high glucose-induced histone hyperacetylation and fibrogenic gene upregulation in mesangial cells. Am J Physiol Renal Physiol 313(2):F423–f429. doi: org/10.1152/ajprenal.00029.2017
19. Zhang HY, Luo GA, Liang QL, Wang Y, Yang HH, Wang YM, Zheng XY, Song XM et al (2008) Neural tube defects and disturbed maternal folate- and homocysteine-mediated one-carbon metabolism. Exp Neurol 212(2):515–521 doi: org/S0014-4886(08)00205-7 [pii] 1016/j.expneurol.2008.04.044
20. Wang L, Wang F, Guan J, Le J, Wu L, Zou J, Zhao H, Pei L et al (2010) Relation between hypomethylation of long interspersed nucleotide elements and risk of neural tube defects. Am J Clin Nutr 91(5):1359–1367 doi: org/ajcn.2009.28858 [pii] 3945/ajcn.2009.28858

21. Goudarzvand M, Afraei S, Yaslianifard S, Ghiasy S, Sadri G, Kalvandi M, Alinia T, Mohebbi A et al (2016) Hydroxycitric acid ameliorates inflammation and oxidative stress in mouse models of multiple sclerosis. Neural Regen Res 11(10):1610–1616. doi: org/10.4103/1673-5374.193240
22. Wang Z, Kim JH, Jang YS, Kim CH, Lee JY, Lim SS (2017) Anti-obesity effect of Solidago virgaurea var. gigantea extract through regulation of adipogenesis and lipogenesis pathways in high-fat diet-induced obese mice (C57BL/6N). Food Nutr Res 61(1):1273479. doi: org/10.1080/16546628.2016.1273479
23. Ismail A, Doghish AS, B E M E, Salama S, A,Mariee AD (2020) Hydroxycitric acid potentiates the cytotoxic effect of tamoxifen in MCF-7 breast cancer cells through inhibition of ATP citrate lyase. Steroids 160108656. doi: org/10.1016/j.steroids.2020.108656
24. Schlett K, Madarasz E (1997) Retinoic acid induced neural differentiation in a neuroectodermal cell line immortalized by p53 deficiency. J Neurosci Res 47(4):405–415
25. Hake SB, Shechter D, Dormann HL, Allis CD (2007) Extraction, purification and analysis of histones. Nat Protoc 2(6):1445–1457. doi: org/10.1038/nprot.2007.202
26. Zhang Q, Xue P, Li H, Bao Y, Wu L, Chang S, Niu B, Yang F et al (2013) Histone modification mapping in human brain reveals aberrant expression of histone H3 lysine 79 dimethylation in neural tube defects.Neurobiology of Disease. ;54404–413. doi: org/S0969-9961(13)00038-7 [pii] 1016/j.nbd.2013.01.014
27. Zhang Q, Bai B, Mei X, Wan C, Cao H, Dan L, Wang S, Zhang M et al (2018) Elevated H3K79 homocysteinylation causes abnormal gene expression during neural development and subsequent neural tube defects. Nat Commun 9(1):3436. doi: org/10.1038/s41467-018-05451-7
28. Xie Z, Dai J, Dai L, Tan M, Cheng Z, Wu Y, Boeke JD, Zhao Y (2012) Lysine succinylation and lysine malonylation in histones. Mol Cell Proteomics 11(5):100–107. doi: org/10.1074/mcp.M111.015875
29. Loeken MR (2005) Current perspectives on the causes of neural tube defects resulting from diabetic pregnancy. Am J Med Genet C Semin Med Genet 135C(1):77–87. doi: org/10.1002/ajmg.c.30056
30. Chi H, Sarkisian MR, Rakic P, Flavell RA (2005) Loss of mitogen-activated protein kinase kinase kinase 4 (MEKK4) results in enhanced apoptosis and defective neural tube development. Proc Natl Acad Sci U S A 102(10):3846–3851. doi: org/10.1073/pnas.0500026102
31. Abell AN, Rivera-Perez JA, Cuevas BD, Uhlik MT, Sather S, Johnson NL, Minton SK, Lauder JM et al (2005) Ablation of MEKK4 kinase activity causes neurulation and skeletal patterning defects in the mouse embryo. Mol Cell Biol 25(20):8948–8959. doi: org/10.1128/MCB.25.20.8948-8959.2005
32. Kawahara A, Che YS, Hanaoka R, Takeda H, Dawid IB (2005) Zebrafish GADD45beta genes are involved in somite segmentation. Proc Natl Acad Sci U S A 102(2):361–366. doi: org/10.1073/pnas.0408726102
33. Zhong J, Reece EA, Yang P (2015) Punicalagin exerts protective effect against high glucose-induced cellular stress and neural tube defects. Biochem Biophys Res Commun 467(2):179–184. doi: org/10.1016/j.bbrc.2015.10.024

34. Bhandari J, Thada PK (2022) Neural Tube Disorders. In StatPearls, StatPearls Publishing Copyright (2022) © StatPearls Publishing LLC
35. Greene ND, Copp AJ (2014) Neural tube defects. Annu Rev Neurosci 37221–37242. doi: org/10.1146/annurev-neuro-062012-170354
36. Hotta K, Takahashi H, Asakura T, Saitoh B, Takatori N, Satou Y, Satoh N (2000) Characterization of Brachyury-downstream notochord genes in the Ciona intestinalis embryo. Dev Biol 224(1):69–80. doi: org/10.1006/dbio.2000.9765
37. Hotta K, Yamada S, Ueno N, Satoh N, Takahashi H (2007) Brachyury-downstream notochord genes and convergent extension in Ciona intestinalis embryos. Dev Growth Differ 49(5):373–382. doi: org/10.1111/j.1440-169X.2007.00935.x
38. Wan C, Liu X, Bai B, Cao H, Li H, Zhang Q (2018) Regulation of the expression of tumor necrosis factor–related genes by abnormal histone H3K27 acetylation: Implications for neural tube defects. Mol Med Rep 17(6):8031–8038. doi: org/10.3892/mmr.2018.8900
39. Chen S, Zhang Q, Bai B, Ouyang S, Bao Y, Li H, Zhang T (2017) MARK2/Par1b Insufficiency Attenuates DVL Gene Transcription via Histone Deacetylation in Lumbosacral Spina Bifida. Mol Neurobiol 54(8):6304–6316. doi: org/10.1007/s12035-016-0164-0
40. Harris MJ, Juriloff DM (2007) Mouse mutants with neural tube closure defects and their role in understanding human neural tube defects. Birth Defects Res A Clin Mol Teratol 79(3):187–210. doi: org/10.1002/bdra.20333
41. Hollander MC, Sheikh MS, Bulavin DV, Lundgren K, Augeri-Henmueller L, Shehee R, Molinaro TA, Kim KE et al (1999) Genomic instability in Gadd45a-deficient mice. Nat Genet 23(2):176–184. doi: org/10.1038/13802
42. Kaufmann LT, Gierl MS, Niehrs C (2011) Gadd45a, Gadd45b and Gadd45g expression during mouse embryonic development. Gene Expr Patterns 11(8):465–470. doi: org/10.1016/j.gep.2011.07.005
43. Sheikh MS, Hollander MC, Fornance AJ Jr (2000) Role of Gadd45 in apoptosis. Biochem Pharmacol 59(1):43–45. doi: org/10.1016/s0006-2952(99)00291-9
44. Takekawa M, Saito H (1998) A family of stress-inducible GADD45-like proteins mediate activation of the stress-responsive MTK1/MEKK4 MAPKKK. Cell 95(4):521–530. doi: org/10.1016/s0092-8674(00)81619-0
45. Miyake Z, Takekawa M, Ge Q, Saito H (2007) Activation of MTK1/MEKK4 by GADD45 through induced N-C dissociation and dimerization-mediated trans autophosphorylation of the MTK1 kinase domain. Mol Cell Biol 27(7):2765–2776. doi: org/10.1128/mcb.01435-06
46. Saha A, Kuzuhara T, Echigo N, Suganuma M, Fujiki H (2010) New role of (-)-epicatechin in enhancing the induction of growth inhibition and apoptosis in human lung cancer cells by curcumin. Cancer Prev Res (Phila) 3(8):953–962. doi: org/10.1158/1940-6207.Capr-09-0247
47. Zhao Z, Reece EA (2013) New concepts in diabetic embryopathy. Clin Lab Med 33(2):207–233. doi: org/10.1016/j.cll.2013.03.017

48. Steinhubl SR (2008) Why have antioxidants failed in clinical trials? Am J Cardiol. ; 101(10a): 14d-19d. doi: org/10.1016/j.amjcard.2008.02.003

Figures

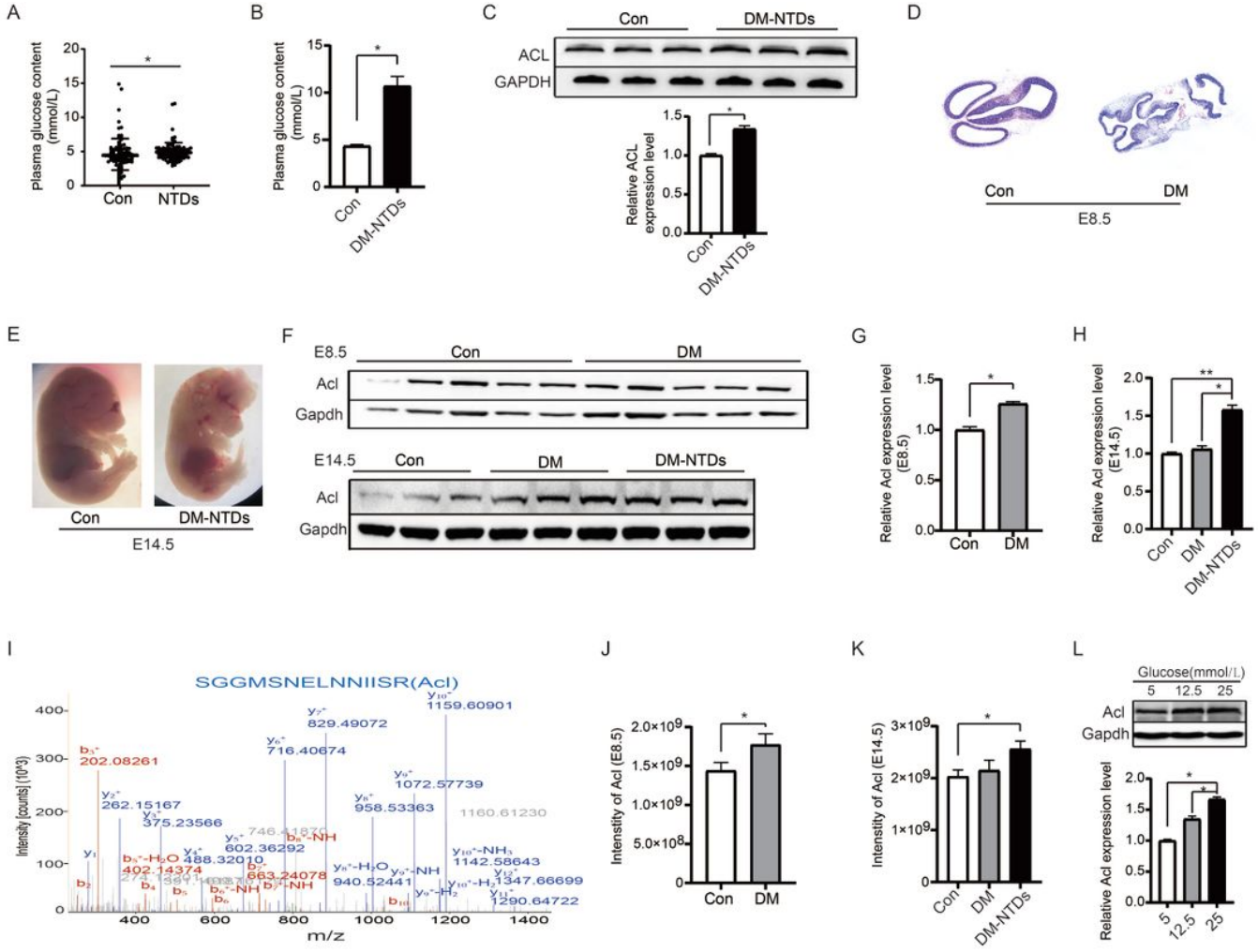

Figure 1

Expression profile of ACL/Acl *in vivo* and *in vitro*. **A** Plasma glucose content in control and NTD-related human maternal samples (n=100). **B** Plasma glucose content in control and DM-NTD for WB validation (n=3). **C** WB assay of ACL protein expression in human control and DM-NTD fetal brain tissues. **D** Hematoxylin-eosin (HE) staining of E8.5 embryos. **E** DM-induced embryonic day 14.5 mouse embryos with typical exencephaly and control mice. **F–H** WB assay of Acl protein expression in brain tissues of E8.5 and E14.5 mice. **I** Typical HPLC-MS/MS spectra of tryptic peptide “SGGMSNELNNIISR” belonging to Acl in E8.5 DM mice. The x- and y-axes represent m/z and relative ion intensity, respectively. **J, K** Quantification of Acl by PRM in E8.5 and E14.5 mice. **L** Acl protein expression assayed by WB in 5, 12.5, and 25 mmol/L glucose-treated NE4C cells. Data are expressed as the mean ± SD, *p < 0.05, **p < 0.01.

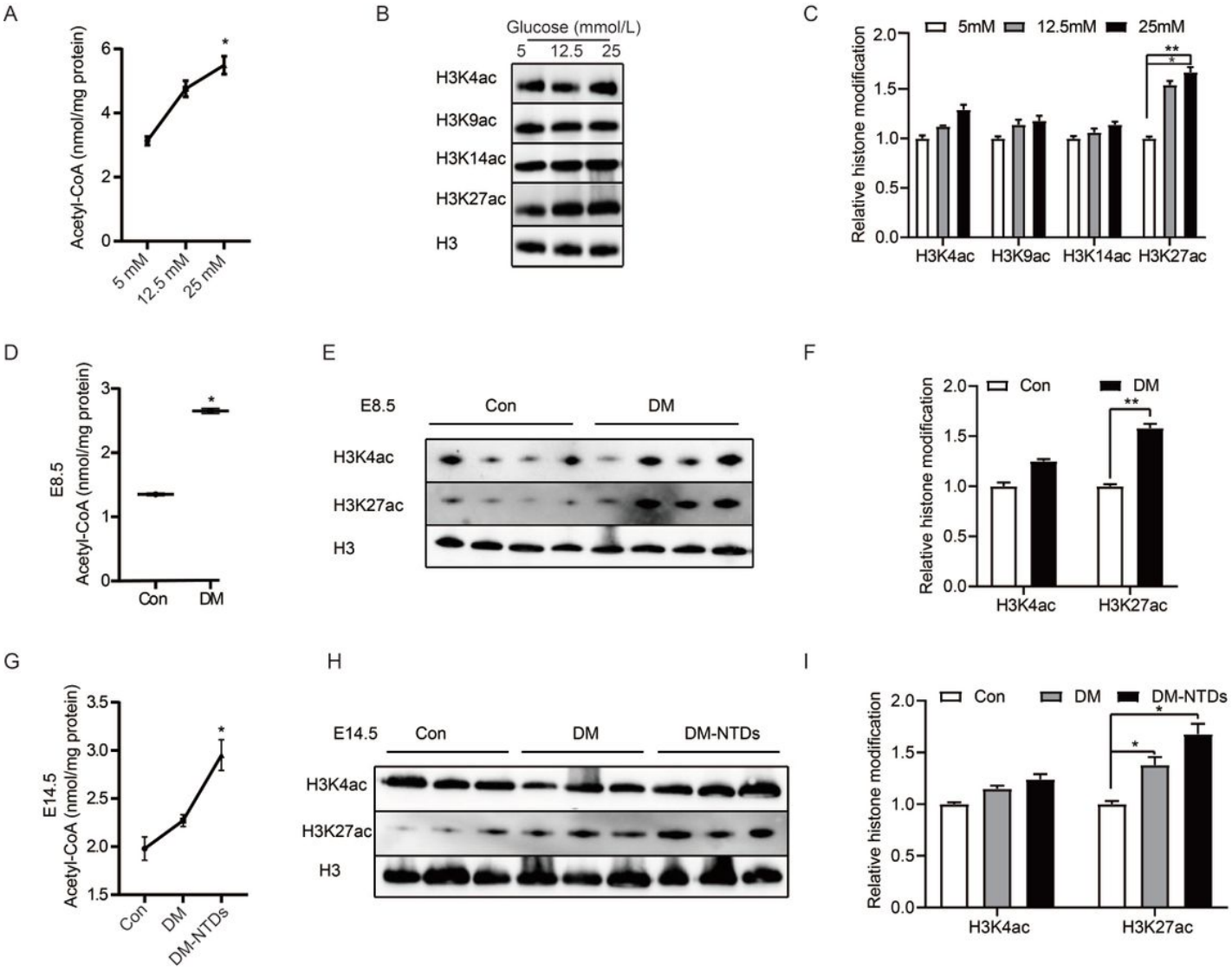

Figure 2

Acetyl-CoA and H3K27ac levels in NE4C cells and DM-induced NTD mouse embryos. **A** Acetyl-CoA levels in NE-4C cells were dose-dependently increased by exposure to 5, 12.5, or 25 mM glucose. **B, C** WB assays of H3K4ac, H3K9ac, H3K14ac, and H3K27ac in cells treated with various concentrations of glucose. **D** Acetyl-CoA level in E8.5 brain tissues. **E, F** WB analysis of H3K4ac and H3K27ac levels in E8.5 brain tissues. **G** Acetyl-CoA level in E14.5 brain tissues. **H, I** WB analysis of H3K4ac and H3K27ac levels in E14.5 brain tissues. Data are expressed as the mean ± SD, *$p < 0.05$, **$p < 0.01$.

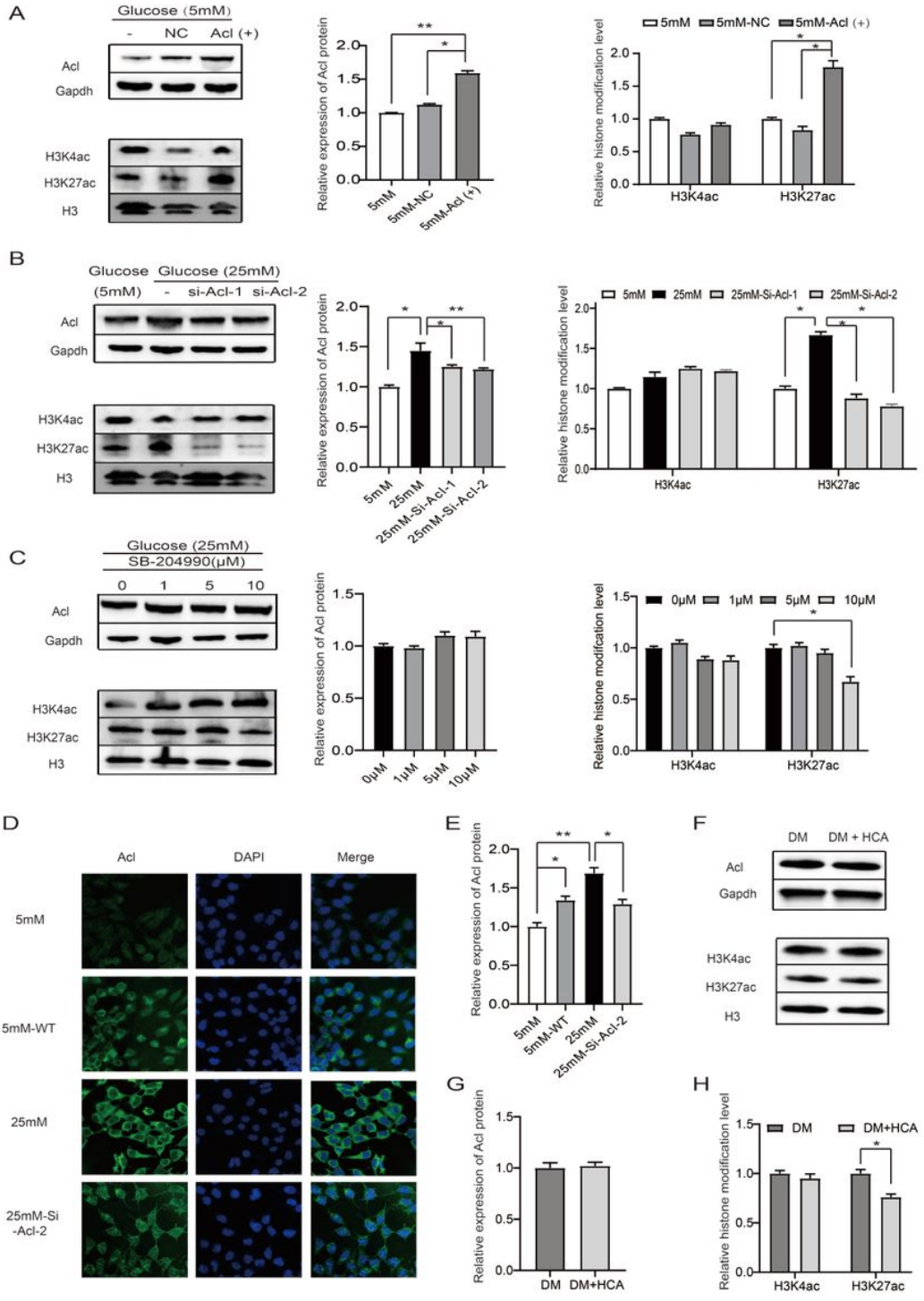

Figure 3

ACL regulates the H3K27ac modification level in NE4C cells and DM-induced NTD mouse embryos. **A** Validation of Acl overexpression in NE-4C cells exposed to 5 mM glucose and the effect on H3K27ac and H3K4ac by WB. **B** Validation of Acl knockdown by shRNA in NE-4C cells exposed to 25 mM glucose and the effect on H3K27ac and H3K4ac by WB. **C** WB was used to measure Acl as well as H3K27ac and H3K4ac levels in 25 mM glucose-treated cells and cells treated with both glucose and ACL drug inhibitor SB-204990 at 1, 5, and 10 μmol/L. **D, E** Immunofluorescence staining confirmed the Acl expression

pattern in Acl-overexpressing or -knockdown cells. **F–H** Level of Acl, H3K27ac, and H3K4ac in E8.5 DM and DM+HCA fetal mice measured by WB. Data are expressed as the mean ± SD, *p < 0.05, **p < 0.01.

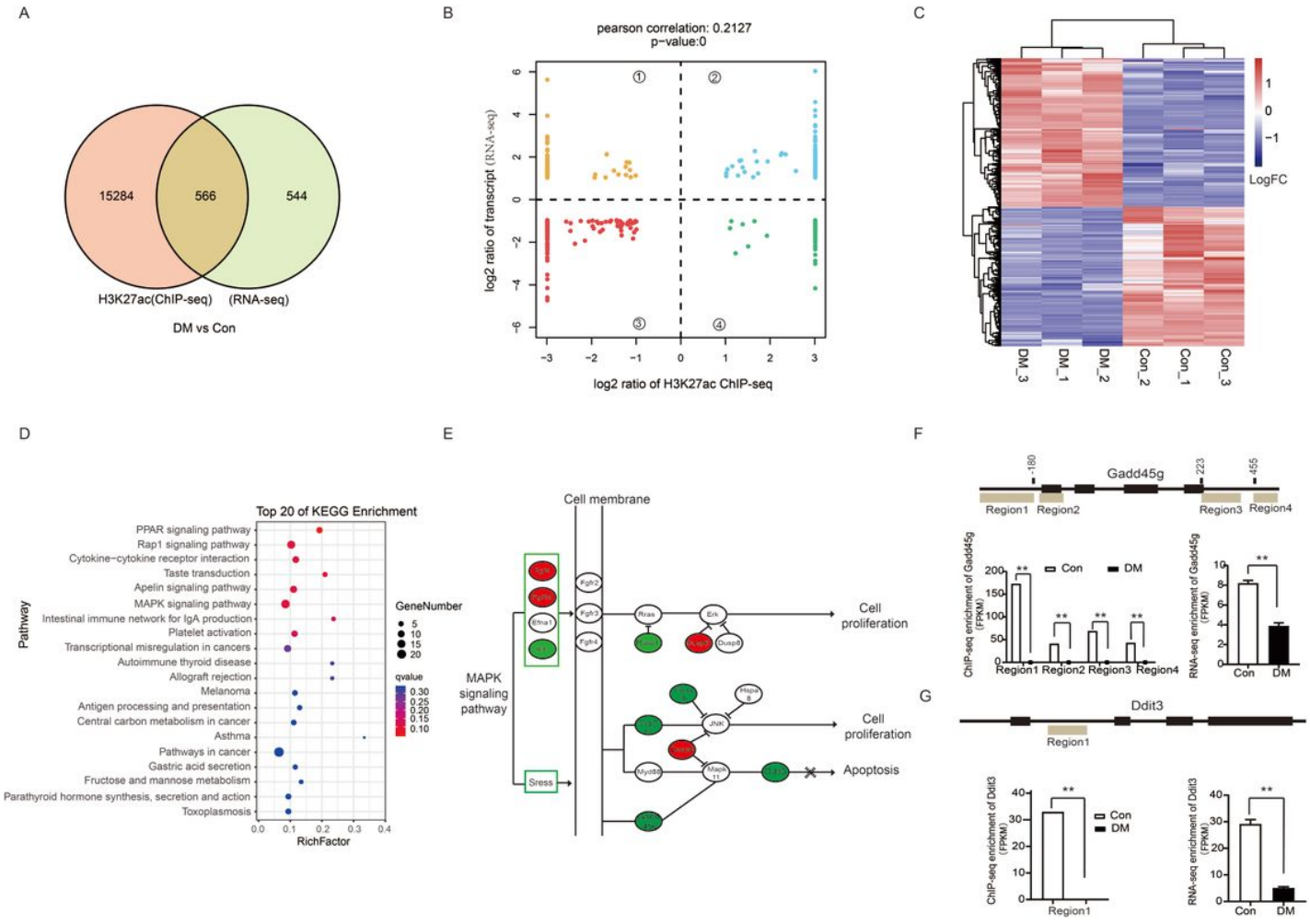

Figure 4

Abnormal H3K27ac regulates decreased expression of NTD genes Gadd45g and Ddit3. **A** Venn diagram of genes with altered expression in RNA-seq and altered enrichment to H3K27ac in ChIP-seq. **B** Four quadrant diagram of the relationship between genes binding to H3K27ac and their expression levels. (1) Genes enriched with H3K27ac were downregulated (>1.2-fold change), while their RNA levels were up-regulated (>1.3-fold change) in the DM group compared with control mice. (2) Genes enriched with H3K27ac were upregulated and their RNA levels were also up-regulated in the DM group compared with control mice. (3) Genes enriched with H3K27ac were downregulated and their RNA levels were also downregulated in the DM group compared with control mice. (4) Genes enriched with H3K27ac were upregulated, while their RNA levels were downregulated in the DM group compared with control mice. **C** Hierarchical clustering of 566 common differentially expressed genes. **D** KEGG pathway results displayed as a bubble chart, showing the top 20 pathways. **E** Altered gene expression of the MAPK pathway. Green indicates downregulated expression in E8.5 DM compared with control mice in RNA-seq and red indicates upregulation**. F, G** ChIP-seq analysis of histone H3K27ac enrichment in various gene regions of Gadd45g (F) and Ddit3 (G) in E8.5 control and DM mice. Data are expressed as the mean ± SD, *p < 0.05, **p < 0.01.

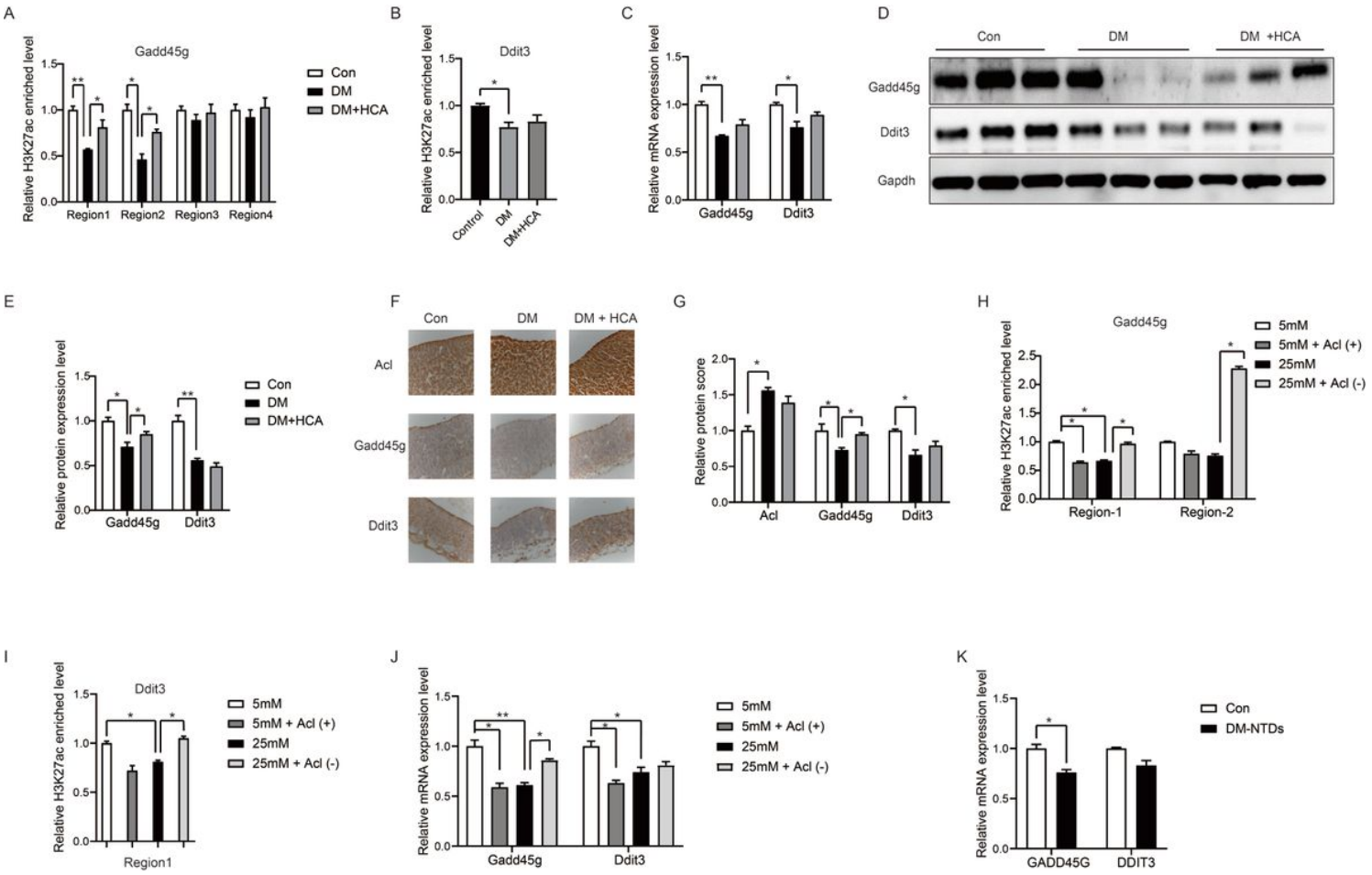

Figure 5

Enhanced Acl regulates Gadd45g/Ddit3 expression by H3K27ac in DM-induced NTDs. **A-B** ChIP-qPCR validated enrichment of various gene regions of Gadd45g (A) and Ddit3 (B) with H3K27ac in E8.5 DM, DM+HCA, and control mice. **C** mRNA levels of Gadd45g and Ddit3 in E8.5 DM, DM+HCA, and control mice were measured by RT-qPCR. **D-E** WB assays of Gadd45g and Ddit3 protein expression in E8.5 mice. **F, G** IHC further validated the protein expression pattern of Acl, Gadd45g, and Ddit3 in E8.5 mice. **H–J** ChIP-qPCR combined with RT-qPCR detected enrichment of various gene regions of Gadd45g and Ddit3 with H3K27ac and their expression levels in Acl-overexpressing or -knockdown NE4C cells. **K** Gadd45g and Ddit3 mRNA levels in control and DM-related NTD human fetal brain tissues were measured by RT-qPCR. Data are expressed as the mean ± SD, *p < 0.05, **p < 0.01.

Supplementary Files

This is a list of supplementary files associated with this preprint. Click to download.

- SupplementaryInformationformanuscript.docx
- SupplementaryTablesS1S5.docx
- TableS6RRMquantificationresultsofAcl.xlsx

- TableS7ChIPseqresultsofH3K27acinE8.5micemodel.xlsx
- TableS8RNAseqresultsofgenesinE8.5micemodel.xlsx
- TableS9IntersectiongenesofChIPseqandRNAseq.xlsx
- TableS10KEGGanalysisresultsof566genes.xlsx